Polymer 51 (2010) 4439–4447

Contents lists available at ScienceDirect

Polymer

journal homepage: www.elsevier.com/locate/polymer

Mechanistic understanding of CO_2-induced plasticization of a polyimide membrane: A combination of experiment and simulation study

Liling Zhang, Youchang Xiao, Tai-Shung Chung*, Jianwen Jiang*

Department of Chemical and Biomolecular Engineering, National University of Singapore, Singapore 117576, Singapore

ARTICLE INFO

Article history:
Received 11 June 2010
Received in revised form
17 July 2010
Accepted 20 July 2010
Available online 29 July 2010

Keywords:
Plasticization
CO_2
Polyimide

ABSTRACT

Experimental measurements and fully atomistic simulations are carried out to examine the CO_2-induced plasticization of a polyimide membrane synthesized from 4,4′-(hexafluoroisopropylidene) diphthalic anhydride (6FDA) and 4,4′-oxydianiline (ODA). With increasing feed pressure, the permeability of CO_2 in the 6FDA-ODA membrane initially decreases, crosses a minimum, and then increases. The plasticization pressure is estimated to be at approximately 8 atm. The radial distribution functions between CO_2 and polyimide atoms reveal that the imide groups are the preferential sorption sites, followed by the ether and CF_3 groups. The experimental and simulated sorption isotherms of CO_2 are in fairly good agreement. At low loadings, CO_2 molecules are largely trapped with small mobility. With increasing loading, the polyimide membrane exhibits a depressed glass transition temperature, a dilated volume and an increased fractional free volume. In addition, larger and more interconnected voids appear and the mean radius of voids increases from 2.5 to 3.3 Å with increasing CO_2 loading. Consequently, the mobility of both CO_2 molecules and polymer chains is enhanced. Based on molecular displacement, the percentages of three types of motions (jumping, trapped, and continuous) are estimated for CO_2 in the membrane. The continuous motion contributes predominantly to CO_2 diffusion. At a high loading, the ether groups in the polyimide chains exhibit a significant effect on plasticization. It is therefore suggested that the plasticization could be suppressed by substituting the ether groups. The microscopic information of this study is particularly useful for the quantitative understanding of plasticization.

1. Introduction

Plasticization is a common phenomenon for polymeric membranes in gas separation processes. Studies have shown that plasticization essentially originates from the interactions between gas and membrane which significantly affect the performance of membrane [1–4]. Plasticization is usually encountered in the separation of natural gas, which involves highly condensable gases such as CO_2, H_2S, H_2O, and hydrocarbons [5–13]. Beyond a critical feed pressure, the permeabilities of both CO_2 and CH_4 increase; consequently, a loss of permselectivity takes place. This undesirable effect is more remarkable in polyimide membranes, despite their good chemical integrity compared to other polymeric membranes.

In the literature, plasticization has been described in a number of ways [14–19]. Due to the complexity, however, most of these descriptions cannot fully address plasticization and associated issues. From a technical point of view, plasticization may be defined as a repertoire of pressure-dependent phenomenon caused by the dissolution of a certain species into polymer matrix that disrupts chain packing and enhances inter-segmental mobility [18]. The pressure at which gas permeability exhibits a minimum is known as the plasticization pressure (P_{plas}). By single-gas permeation and sorption measurements, CO_2-induced plasticization was examined in 11 different glassy polymers and a relationship was proposed between plasticization pressures and the chemical/physical properties of polymers [17]. Nevertheless, the general permeability–pressure relationship is inadequate to determine the incipient point of plasticization which is strongly time-dependent [20], and several issues are associated intimately with plasticization [21]. For example, the dilation and swelling of polysulfone and poly(ethylmethacrylate) films were observed by measuring the dimensional changes upon the sorption of high-pressure CO_2 [15,22]. Glass transition temperature (T_g) is related with the stiffness of polymer chain; therefore, the depression of T_g is also an evidence for plasticization. The 6FDA-based polyimides were reported to show a large T_g depression of 198 °C when CO_2 feed pressure reached 50 bar [23]. Moreover, it has been found that the depression of T_g could even occur below the apparent plasticization pressure [16]. CO_2-induced plasticization is dependent on membrane thickness as observed from accelerated plasticization in ultra-thin

* Corresponding authors.
E-mail addresses: chencts@nus.edu.sg (T.-S. Chung), chejj@nus.edu.sg (J. Jiang).

0032-3861/$ – see front matter © 2010 Elsevier Ltd. All rights reserved.
doi:10.1016/j.polymer.2010.07.032

polyimide films [24]. Temperature-dependent CO_2-induced plasticization at different operating temperatures revealed that plasticization is more pronounced at lower temperatures [25]. A few studies have been conducted to determine the onset of plasticization. One example was to examine the absolute heat of sorption as a function of pressure. The onset of plasticization was proposed corresponding to the pressure at which the heat of sorption changed sign (from negative to positive) [26]. Another attempt was to relate plasticization to the concentration of CO_2 dissolved in polymer [17,27]. It was suggested that all polymers are swollen at approximately the same CO_2 concentration, which is reached at different pressures [27].

The fundamental understanding of CO_2-induced plasticization is crucial to the enhancement of separation efficacy and the development of high-performance polymeric membranes. The ever-growing computer technology and the recent advances in molecular modeling have provided a unique opportunity to examine plasticization [28]. The microscopic insight at a molecular level is indispensable in quantitatively unraveling the underlying physics. To date only few simulation studies have been reported to investigate plasticization in polymeric membranes. The sorption isotherms of CO_2 were simulated in a hypothetical glassy polymer with T_g around 500 K [29]. Since CO_2-induced swelling of glassy polymer is a complex process involving the interplay of sorption and dilation, it is formidable to directly simulate the time-evolution of plasticization. The atomistic packing models were constructed for unswollen polysulfone (PSU) and poly(ether sulfone) (PES) at ambient conditions, also for swollen PSU and PES at experimentally observed CO_2 swelling pressure (50 bar). The sorption isotherms were subsequently estimated by interpolating two isotherms in the unswollen and swollen polymers [30–32]. CO_2 sorption and swelling in atactic polystyrene were simulated over temperatures ranging from 308 to 405 K at pressures up to 300 bar [33].

The question remains elusive whether there is a physical property of significance indicating the critical threshold of plasticization. In this paper, a combined experimental and simulation study is reported for CO_2-induced plasticization in a membrane with different CO_2 loadings at 308 K. The membrane considered is 6FDA-ODA polyimide (6FDA = 4,4′-(hexafluoroisopropylidene) diphthalic anhydride, ODA = 4,4′-oxydianiline), one of most commonly studied glassy polymers due to its high permeability and selectivity for CO_2. The bulky $-C(CF_3)_2$ groups in 6FDA-based polyimide membranes have two important effects: (1) inhibit efficient chain packing, thus create a large free volume and increase permeability; (2) increase chain stiffness, restrict chain mobility and enhance selectivity. The sorption and diffusion of CO_2 in the 6FDA-ODA membrane were measured experimentally and evaluated by fully atomistic simulations. The fractional free volume and its distribution, glass transition temperature, sorption isotherm, dynamics of polymer chains and penetrants are comprehensively investigated as a function of CO_2 loading from simulations. In comparison between experimental and simulated findings, we aim to achieve a quantitative understanding of the relation among polymer structure, its interaction with CO_2 and its performance, which could assist in the rational design of next-generation polymeric materials for high-efficacy gas separation.

2. Experimental materials and methods

2.1. Materials

The reagents 4,4′-(hexafluoroisopropylidene) diphthalic anhydride (6FDA), and 4,4′-oxydianiline (ODA), supplied from Sigma–Aldrich, were purified by vacuum sublimation before usage. NMP (N-methyl-pyrrolidone) purchased from Merck, was distilled at 42 °C under 1 mbar after drying with molecular sieve before use. Other chemicals and solvents such as acetic anhydride, triethylamine and methanol were all reagent grades or better from Aldrich and were used without further purification. The purity of CO_2 was 99.99%.

2.2. Polyimide synthesis

Chemical imidization was performed during the synthesis of polyimide. A stoichiometric amount of 6FDA was added to an ODA's NMP solution at a designated molar ratio in a moisture free flask with stirring and nitrogen inlet at room temperature. After reaction for 24 h, a high molecular weight polyamic acid was formed, and then a mixture of acetic anhydride and triethylamine at 4:1 M ratio was slowly added to the polyamic acid solution for imidization for 24 h. After precipitation in methanol, the polymer was filtered, washed and dried under 150 °C in vacuum for 24 h.

The molecular weights of the modified polyimide were determined by gel-permeation chromatography (GPC) measurements, which were carried out on an HP 1100 HPLC system equipped with the HP 1047A RI detector and Agilent 79911GP-MXC columns. Tetrahydrofuran was used as the solvent and the flow rate was controlled at 1.0 ml/min. The polymer was dissolved in tetrahydrofuran at a concentration of 0.005 wt%. The molecular weights were estimated by comparing the retention times in the column to those of poly(styrene) standards.

2.3. Membrane preparation and characterization

Polyimide solutions at a concentration of 2% (w/w) were prepared by dissolving the readily-soluble polymer powders in dichloromethane. The solutions were then filtered using Whatman's filters (1 μm) to remove insoluble materials and dust particles. Then the solutions were cast onto silicon wafers at ambient temperature. Dense membranes were formed after most of the solvent was allowed to evaporate slowly over a period of about 5 days. The residual solvent was removed by placing the dense membranes in a vacuum oven at 250 °C. All membranes were cut into circles with a diameter of 38 mm. Only the membranes with a thickness of about 50 ± 5 μm were used in the subsequent measurements.

The permeability of CO_2 was determined by a constant volume and variable pressure method. The testing temperature was 35 °C and pressure was increased gradually from 1 atm to 30 atm. The rate of downstream pressure increase (dP/dt) at a steady state was used to calculate the gas permeability using following equation:

$$P = \frac{273 \times 10^{10}}{760} \frac{VL}{AT(p_2 \times 76/14.7)} \left(\frac{dp}{dt}\right) \quad (1)$$

where P is the permeability of a membrane in Barrer (1 Barrer = 10^{-10} cm^3(STP)cm/(cm^2 s cmHg), V is the volume of the downstream chamber (cm^3), L refers to the thickness of the membrane (cm), A is the effective area of the membrane (cm^2), T is the operating temperature (K), and the pressure of the feed gas in the upstream is given by p_2 (psia).

The equilibrium isotherm of CO_2 was measured at 35 °C using a Cahn D200 microbalance sorption cell. Prior to test, the microbalance was calibrated using the testing gas at various pressures, the weight gained was plotted as a function of pressure. The system was evacuated for at least 24 h before loading the sample (50–100 mg) into the sample pan. The testing gas was fed into the system at a desired pressure and the gas was absorbed by the polymer matrix until it reached a state of equilibrium. The weight gain was recorded and the same steps were repeated to test the next pressure, the system was not evacuated until the end of the test. The sample pan was tared to zero under vacuum at each time when starting a new sample. The sorption coefficient was calculated by considering the buoyancy force of the polymer in CO_2.

3. Atomistic model and simulation protocol

The 6FDA-ODA polyimide (PI) membrane was constructed atomistically by the Theodorou/Suter method in the Amorphous Cell of Materials Studio [34]. The model consisted of one PI chain with 72 repeat units and 4180 atoms in a three-dimensional periodic cell. The initial packing density was 0.1 g/cm^3 and gradually compressed to a target density of 1.4 g/cm^3. To reduce the possible packing artifacts such as ring catenations and spearing of the PI chain during compression, 100 N-Methyl-2-pyrrolidone (NMP) molecules were added randomly into the cell as obstacles. After reaching the target density, the NMP molecules were removed. Then the model membrane was subjected to extensive equilibration procedures consisting of energy minimization, stimulated compression and annealing, finally a long molecular dynamics (MD) simulation in a NPT ensemble (constant number of molecules, pressure, and temperature) with temperature and pressure of 308 K and 1 atm. The equilibrated density of the PI membrane was 1.40 g/cm^3, fairly close to the experimental value (1.43 g/cm^3) [35]. Accurate prediction of membrane density requires not only a good force field, but also a well-equilibrated model. In addition, polymer chain length is another factor that may affect density. A model with short polymer chains usually gives a smaller density and a larger fraction of free volume due to finite chain-length effect. The weight-average molar mass of the 6FDA-ODA membrane was experimentally determined as 48,000 g/mol. However, the model membrane in the simulation has a mass weight around 43,800 g/mol, which is 8.8% lower than the experimental value. This could contribute to the slightly lower density predicted from simulation. We note that for typical glassy polymer membranes, the deviations between simulated and experimental densities could be up to 4% [28,36]. Here the deviation for the 6FDA-ODA membrane is about 2%, implying the accuracy of the model and force filed used in our simulation.

At the maximum gas pressure (20 atm) in our experiments, the measured CO_2 loading in the PI membrane is 52.5 [cm^3 (STP)/cm^3 polymer], approximately corresponding to 80 CO_2 molecules in the simulation cell. To examine the effect of CO_2 loading, a series of PI/CO_2 systems were constructed with 5, 10, 20, 40, and 80 CO_2 molecules, respectively. CO_2 molecules were added into the equilibrated model membrane at random positions using the Sorption of Materials Studio [34]. If CO_2 molecules and PI atoms overlapped, the insertion was rejected and a new position was attempted. Each PI/CO_2 system was energetically minimized using three different methods: (a) conjugate gradient minimization, (b) programmed minimization combining conjugate gradient minimization with a MD search, and (c) a zero temperature MD simulation. Thereafter, the configuration of the lowest energy was chosen for a cycle of annealing process, followed by 0.5 ns NVT (constant number of particles, temperature, and volume) MD simulation at 308 K. Finally, 2 ns NPT MD simulation was performed at 308 K and 20 atm. The cell volume and system energy were found to fluctuate slightly around well-defined averages over the 2 ns duration, indicating that the system reached equilibration. As discussed below, upon the dissolution of CO_2 molecules, the physical properties of the polymer matrix were found to change substantially.

To characterize the constructed PI matrix in the absence or presence of CO_2, the glass transition temperature T_g, fractional free volume and void distribution, as well as the dynamics of PI and CO_2 were calculated. For a given system, T_g was determined by the system volume as a function of temperature. The volume was obtained from a series of subsequent MD runs, in which the temperature was quenched from 808 to 308 K with 10 K intervals at constant pressure. At each temperature, the system was equilibrated for 100 ps and the average volume was determined from 50 ps production. We found the volume remained nearly the same in longer MD runs. For PI in the absence of CO_2, the pressure was chosen at 1 atm for comparison with experimental condition; while for PI/CO_2 systems, the pressure was 20 atm to study the effect of CO_2 loading. It was found that the pressure had an insignificant effect on the volume and density of the system. The mobility of PI and CO_2 were estimated by calculating the molecular displacements from MD simulation in NVT ensemble. Starting with the equilibrated configuration mentioned above, another 2 ns MD simulation was carried out and followed by 18 ns production run. The displacements were calculated from the time averages of the trajectories.

The fraction free volume (FFV) and void distribution were estimated by Monte Carlo (MC) simulations. A probe was randomly inserted into the simulation cell and the insertion was considered to be successful if the probe did not overlap with any polymer atom. The ratio of successful insertions to the total number of insertions gave the FFV. In this study, the probe used had a radius of 1.0 Å. The void distribution was estimated by a method previously used for micro-crystalline materials [37,38]. Specifically, the simulation cell was divided into three-dimensional fine grids with a size of approximately 0.1 Å. The void size at a grid was determined as the diameter of the maximum cavity that encloses the grid and additionally has no overlap with any polymer atom. To determine the FFV and void distribution of the swollen PI matrix in a PI/CO_2 system, all CO_2 molecules were removed and the cell volume was kept unchanged.

In our simulations, the polymer consistent force field (PCFF) [39,40] was used. The PCFF consists of bond stretching (E_b), bending (E_θ), torsion (E_ϕ), out-of-plane bending (E_χ), Lennard-Jones 6–9 (E_{LJ}), and Coulombic potentials (E_{Coul}),

$$\begin{aligned} E_{\text{total}} &= E_b + E_\theta + E_\phi + E_\chi + E_{\text{elec}} + E_{LJ} \\ &= \sum_b \left[k_2^b (b-b_0)^2 + k_3^b (b-b_0)^3 + k_4^b (b-b_0)^4\right] \\ &+ \sum_\theta \left[k_2^\theta (\theta-\theta_0)^2 + k_3^\theta (\theta-\theta_0)^3 + k_4^\theta (\theta-\theta_0)^4\right] \\ &+ \sum_\phi [V_1(1-\cos\phi) + V_2(1-\cos 2\phi) + V_3(1-\cos 3\phi)] \\ &+ \sum_\chi k^\chi (\chi-\chi_0)^2 + \frac{1}{4\pi\varepsilon_0}\sum_{i,j}\frac{q_i q_j}{r_{ij}} + \sum_{i,j}\varepsilon_{ij}\left[2\left(\frac{r_{ij}^0}{r_{ij}}\right)^9 - 3\left(\frac{r_{ij}^0}{r_{ij}}\right)^6\right] \end{aligned} \tag{2}$$

where b, θ, ϕ and χ represent bond length, bond angle, dihedral angle or out-of-plane angle formed by pairs, triplets and quadruplets, respectively; ε_0 is the permittivity of vacuum, q_i the atomic charge on atom i, and r_{ij} is the distance of between atoms i and j; ε_{ij} and r_{ij}^0 are the well depth and collision diameter of the LJ potential, respectively. The cross-terms have small contributions and were not included.

All the MD simulations were performed with DL_POLY package [41,42] using an in-house developed code to convert the structure files created by Materials Studio. The computation speed with DL_POLY was one to two orders of magnitude faster than Materials Studio. The initial velocities were assigned using the Maxwell–Boltzmann distribution at the desired temperature (308 K). The dispersive interactions were evaluated by the atom-based method with a spherical cutoff of 12.5 Å and the Coulombic interactions were estimated by the Ewald sum with an accuracy of 10^{-6}. The temperature and pressure were controlled by the Nosé-Hoover method with a relaxation time of 0.8 ps. The equations of motion were solved by the velocity Verlet algorithm. The time step was 1 fs and trajectory was stored every 1 ps. GCMC simulations for sorption isotherms of CO_2 were carried out using the Sorption module in Materials Studio [34]. Because the chemical potentials of adsorbate

in adsorbed and bulk phases are identical at thermodynamic equilibrium, the GCMC simulation allows one to relate the chemical potentials of adsorbate in both phases and has been widely used to simulate adsorption. The Metropolis algorithm was used to govern the trial moves of CO_2 molecules, including rotation, translation, insertion, and deletion. The number of trial moves in a typical GCMC simulation was 1.6×10^7, in which the first half were used for equilibration and the second half for ensemble averages.

4. Results and discussion

4.1. Experimental permeability, solubility, and diffusivity

Fig. 1 shows the experimental permeability P, solubility coefficient S, and diffusion coefficient D of CO_2 in the 6FDA-ODA membrane at 35 °C. The P and S were measured by gas permeation cell and microbalance, respectively; and the D was calculated based on the solution-diffusion mechanism $D = P/S$. As pressure increases, S decreases monotonically. The reason is that sorption in a membrane occurs initially at the strongest sites and then at relatively weaker sites with increasing pressure. In contrast, the D increases monotonically over the pressure range in this study. Generally, D decreases with increasing penetrant loading due to steric hindrance. The observed increase of D as a function of CO_2 loading in the PI membrane is attributed to two simultaneous processes: (1) CO_2 is preferentially sorbed at the strongest sites at low loadings, which retards the mobility of CO_2. With increasing CO_2 loading, the strongest sites are saturated and CO_2 tends to sorb at relatively weaker sites; as a consequence, the mobility increases. (2) CO_2 diffuses in the PI matrix by molecular hopping through the transient opening of free volume due to thermal fluctuations. The distribution of free volume in the PI/CO_2 system depends primarily on the packing and motion of PI segments, in addition to CO_2 sorption. The relation between the diffusion coefficient D of a hard-sphere fluid and the free volume in a glassy membrane was proposed by Cohen and Turnbull: $D = A\exp(-\gamma v^*/v_f)$, where v^* is the critical volume of gap opening to allow a diffusive jump, v_f is the average free volume per sorbed molecule, and A and γ are constants [43]. The mobility of local chain segments near a diffusing penetrant is related to penetrant loading. At a higher CO_2 loading, the polymer matrix is swollen to a larger degree and contains more free volume; therefore, the diffusion coefficient of CO_2 increases.

As a consequence of the opposite trend of the solubility and diffusion coefficients with increasing pressure, the permeability of CO_2 in the PI membrane exhibits non-monotonic behavior. With increasing pressure, the permeability initially decreases, passes a minimum, and then increases. The minimum occurs at approximately 8 atm of CO_2 pressure, which is conventionally referred to as the "plasticization pressure". It is intriguing to question what takes place in the polymer matrix with increasing CO_2 pressure up to 8 atm. Plasticization is a time-dependant phenomenon and it is a formidable task to unravel the detailed mechanism experimentally. As shown below, however, molecular simulation could provide the microscopic insight into the interactions of CO_2-polymer, the free volume distribution, the dynamics of CO_2 and polymer chain, and other important information.

4.2. Interactions of CO_2-polymer

The radial distribution function $g(r)$ represents the probability of finding a pair of atoms at a distance r with respect to the bulk phase in a completely random distribution. It is defined by ensemble average

$$g_{AB}(r) = \frac{1}{\rho_{AB} 4\pi r^2} \frac{\sum_{t=1}^{K} \sum_{j=1}^{N_{AB}} \Delta N_{AB}(r \to r + \delta r)}{N_{AB} \times K} \quad (3)$$

where N_{AB} is the total number of atoms A and B in the system, K the number of time steps, δr the distance interval, ΔN_{AB} the number of B (or A) atoms between r to $r + \delta r$ around an A (or B) atom, and ρ_{AB} the bulk density. Generally, the location of a peak in $g(r)$ can be used to identify the nearest interaction distance and provide a microscopic picture of the local interatomic environment. Fig. 2 shows the $g(r)$ of CO_2 around four typical atoms of the PI chain; namely, the oxygen and nitrogen in imide, the fluorine in $-CF_3$ group, and the oxygen in ether (defined as O1, N1, F, and O2 in the inset, respectively). Note that the system for Fig. 2 contains 10 CO_2 molecules in the simulation cell. The pronounced peaks are observed in the $g(r)$ of CO_2–O1 and CO_2–N1 at 3.5 and 5.4 Å, respectively. This implies that the O1 and N1 atoms in imide are the preferential sorption sites for CO_2. The O2 atoms are relatively weak as seen from the $g(r)$ of CO_2–O2 which exhibits lower peaks at longer distances, because the O2 atoms are restricted between two phenyl rings and not readily accessible by sorbate molecules. There is no distinct peak in the $g(r)$ of CO_2–F; therefore, the F atoms have the least interaction with CO_2. The reason is that the bulky $-CF_3$

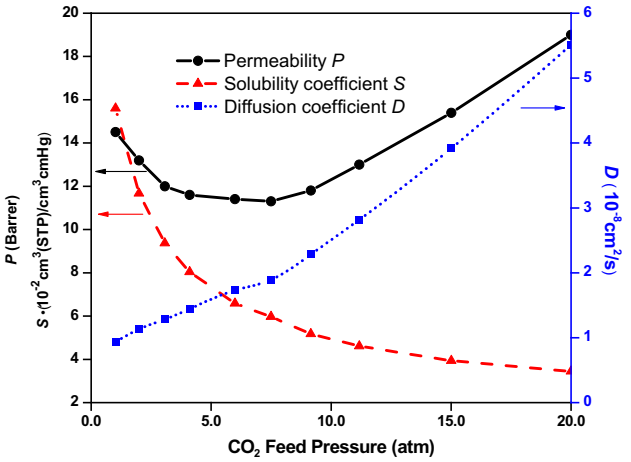

Fig. 1. Experimental permeability, solubility, and diffusion coefficients of CO_2 in 6FDA-ODA polyimide membrane at 35 °C.

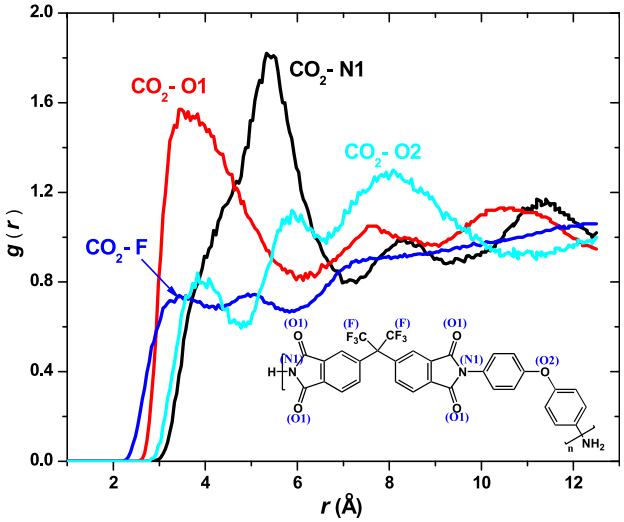

Fig. 2. Radial distribution functions $g(r)$ of CO_2 around O1, N1, F, and O2 atoms of PI chain (indicated in the inset) at a loading of 10 CO_2 molecules in the simulation cell.

group creates a relatively large local void and the potential field around is not strong.

The interaction sites may shift with loading and the loading-dependence is different for various atoms. As shown in Fig. 3, the peak height in the $g(r)$ of CO_2–O1 drops as CO_2 loading increases from 10 to 80, similar behavior is also observed for CO_2–N1 (not shown). This is because that O1 and N1 in imide are the preferential interaction sites, at which CO_2 binds initially. With increasing CO_2 loading, these sites become more or less saturated and CO_2 starts to bind at the less preferential sites such as F and O2 atoms. It is particularly obvious for the F atoms in Fig. 3b. At a low loading of 10 CO_2 molecules, no distinct peak is observed around the F atoms; however, a sharp peak appears at 3.7 Å when the loading is 20. Upon further increase of loading to 40 and 80, the peak height drops as seen in Fig. 3a; implying the F atoms are fully bound with CO_2 molecules. For the O2 atoms in Fig. 3c, because of the steric hindrance of two phenyl rings, the peak at short distance is not pronounced at a low CO_2 loading. With increasing CO_2 loading from 10 to 40, the overall intensity of $g(r)$ increases only slightly. At a high loading of 80, however the peak at 5.6 Å becomes substantially structured. This is because the increasing interactions between CO_2 and O2 atoms in ether groups lead to a less inter-segmental rigidity and more flexible polymer chains, which in turns reduce the steric hindrance for CO_2 to interact with the ether groups.

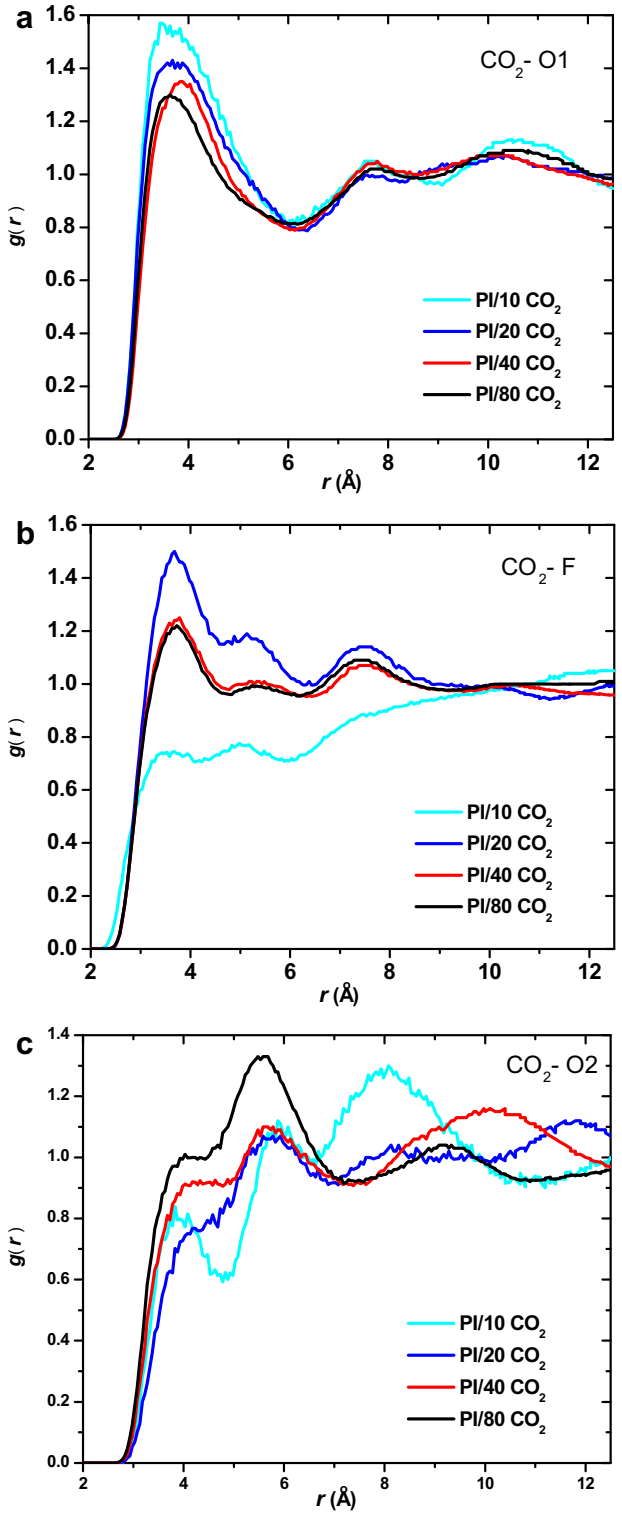

Fig. 3. Radial distribution functions $g(r)$ of CO_2 around O1, F, and O2 atoms respectively in PI/CO_2 systems at different CO_2 loadings with 10, 20, 40, and 80 CO_2 molecules in the simulation cell.

As will be discussed below, the PI/CO_2 systems show stronger plasticization upon loading variation from 40 to 80 CO_2 molecules. The $g(r)$ of CO_2–O1 and CO_2–F in Fig. 3(a–b) almost converge at CO_2 loadings of 40 and 80. The convergence suggests that the interactions of CO_2 with O1 (also N1) and F atoms exert an insignificant effect on plasticization. It is reasoned that upon sorption at the imide and CF_3 groups, CO_2 molecules point along the direction of the lone pair electrons in the O1 and F atoms, thus are located a bit away from the PI backbone and do not strongly affect the dynamics of PI chain. In contrast, the $g(r)$ of CO_2–O2 in Fig. 3c behaves in a different way because it changes pronouncedly as loading increases from 40 to 80. The lone pair electrons in the O2 atoms are conjugated with the inter-segmental phenyl rings, and the charge-transfer between the phenyl rings is reduced when CO_2 binds at the O2 atoms. Therefore, the rotation of the oxygen-phenyl bonds is more favorable resulting in a more flexible PI chain. This reveals that the interactions between CO_2 and ether groups may promote plasticization in the PI membrane.

4.3. Glass transition temperature, volume dilation, and free volume distribution

The penetrant-induced glass transition temperature (T_g) depression and volume dilation are known to occur during CO_2 sorption in glassy polymers [22,23]. Fig. 4 shows the cell volumes of PI and PI/CO_2 systems at different CO_2 loadings. A distinct kink in each curve indicates the occurrence of glass transition. T_g of PI in the absence of CO_2 is approximately 589 K, which is slightly higher than experimentally determined 573 K [35]. A plausible reason could be that the quench rate in our simulations was typically 10 orders of magnitude faster than in experimental measurements. The estimated T_g's of PI/CO_2 systems are 583, 582, 571, 543, 522 K with CO_2 loadings of 5, 10, 20, 40, and 80, respectively. The depression of T_g with increasing CO_2 loading is because the sorbed CO_2 enhances the mobility of polymer chains. With 80 CO_2 molecules sorbed ($\sim$50 cm^3 (STP)/cm^3), T_g is reduced by 67 °C, which is in accord with the reduction of 40–50 °C experimentally reported at a CO_2 concentration of 40 cm^3 (STP)/cm^3 [44].

The volume dilation induced by CO_2 was estimated by comparing the system volumes with that in the absence of CO_2. Table 1 summarizes the relative volume dilation of PI at different CO_2 loadings at 308 K. The volume dilation is small at a low CO_2 loading, but gradually increases at higher loadings. This is because at a low loading CO_2 molecules fill the existing voids around the preferential sorption sites in the polymer matrix. Only after

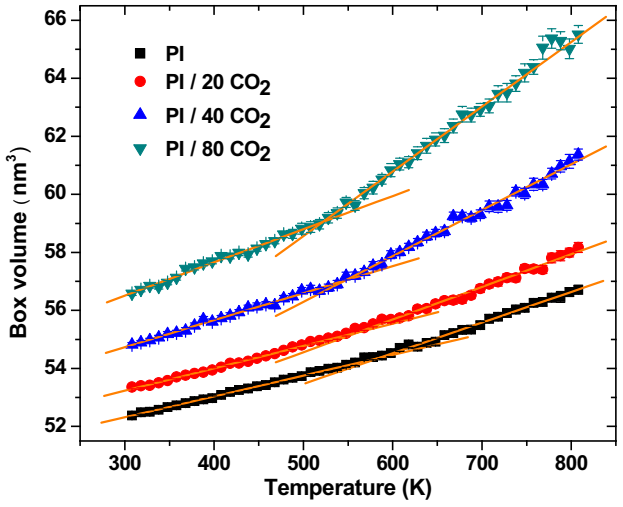

Fig. 4. Volume of simulation cell as a function of temperature in PI and PI/CO_2 systems at different CO_2 loadings with 10, 20, 40, and 80 CO_2 molecules in the simulation cell.

a critical loading of 40 CO_2 molecules, the polymer matrix is swollen by sorbed CO_2 and the volume is dilated; consequently, we may infer this critical loading as the onset of plasticization. With 80 CO_2 molecules sorbed [52.5 cm^3(STP)/cm^3 polymer], the relative volume dilation is 8.2%. This is consistent with a recent simulation study, in which a value of 8.6% was predicted for poly(ether sulfone) at CO_2 concentration of 56.5 cm^3(STP)/cm^3 [31].

The size and distribution of free volume in polymer membranes play a substantially important role in sorption and diffusion of gas species. The fractional free volume (FFV) estimated is given in Table 1 for each system. As CO_2 loading increases, the FFV rises because of the CO_2-induced volume dilation and the increased void size in polymer matrix. Fig. 5 illustrates the morphology of free volume in the PI and PI/CO_2 systems. In the absence of CO_2 or at a low CO_2 loading, the free volume is dominated by a collection of small voids. At a high CO_2 loading, however, large voids appear and some are interconnected. A detail analysis for the distribution of void size is shown in Fig. 6. The voids in PI in the absence of CO_2 are narrowly distributed with radius $<$ 1.6 Å. It is significant to note with increasing CO_2 loading, there are less voids with radius $<$ 1.6 Å but more voids with radius $>$ 1.6 Å. CO_2 has a kinetic radius 1.65 Å; therefore, the void size would be larger than 1.6 Å upon CO_2 sorption and this trend becomes more dominant with more CO_2 sorbed. In particular, only $\sim$ 1% of the voids have radius $>$2.4 Å at a low CO_2 loading and the percentage increases to 4% and 9% with 40 and 80 CO_2 molecules. The mean radius of the voids ranges from 2.5 to 3.3 Å with increasing CO_2 loading in the system.

4.4. Sorption of CO_2

As mentioned above, the CO_2 molecules in the PI/80CO2 system were removed after equilibration. GCMC simulation was subsequently carried out to estimate the sorption isotherm of CO_2 in this dilated PI matrix. As shown in Fig. 7, the simulated loading at 20 atm and 308 K was slightly higher than the experimental value. This was also observed in the simulated isotherms in the PSU55 model membrane [31]. This discrepancy implies that a much longer time is needed in experiments to reach sorption equilibrium at a high pressure. Also shown in Fig. 7 is the isotherm from simulation in the PI membrane without considering the volume change. The simulated isotherms of CO_2 in the PI and dilated PI matrixes were fitted to the dual-mode sorption model

$$C(P) = K_H P + C^{\circ}\frac{bP}{1+bP} \tag{4}$$

where K_H is the solubility coefficient in the Henry regime and C° is the saturation constant and b is the affinity constant.

To predict the isotherm taking into account the volume dilation, a simple interpolation was used by assuming a linear change between solubility and membrane density [31]

$$C(P) = \left(1-\frac{P}{P_{PI/80CO_2}}\right)C_{PI}(P) + \left(\frac{P}{P_{PI/80CO_2}}\right)C_{PI/80CO_2}(P) \tag{5}$$

where $P_{PI/80CO_2}$ is the pressure 20 atm at which the PI/80CO_2 system was constructed to represent the experimental dilated state. $C_{PI}(P)$ and $C_{PI/80CO_2}(P)$ are the loadings as functions of pressure in the PI and PI/80CO_2 systems, respectively. It is seen that the experimental and simulated isotherms agree fairly well. At high pressures, the simulated extent of sorption was larger than the experimental measurement, as a consequence of several plausible factors. First, the sorption process in simulation is fundamentally different from that in experiments. In the former, CO_2 molecules are directly inserted into the favorable sites in the polymer matrix. In the latter, however, CO_2 enters the membrane from the feed side and then dissolves. Therefore, the rates reaching a steady state are not the same in the simulation and experiment. Second, the time scale involved is also significantly different. In practice, plasticization is a time-dependent phenomenon and varies with time; while sorption simulation by the GCMC method does not include the time-evolution effect and is based on the well-equilibrated polymer matrix. Third, the flexibility of polymer chains is incorporated in the MD simulation for the dynamics of PI chains and CO_2 molecules, but not in the GCMC for sorption. Finally, the assumption for the linear change between solubility and density may not be accurate. All these factors come into play and lead to the deviations between predicted and experimental isotherms. Therefore, a more sophisticated simulation is desired by incorporating these factors to improve the prediction of sorption isotherm.

Table 1
Simulated cell length, volume dilation, and fractional free volume (FFV) in PI and PI/CO_2 systems at different CO_2 loadings at 308 K. The probe radius used to calculate FFV was 1.0 Å.

	PI	PI/5 CO_2	PI/10 CO_2	PI/20 CO_2	PI/40 CO_2	PI/80CO2
Cell length (Å)	37.41	37.44	37.48	37.57	37.98	38.40
Volume dilation	–	0.3%	0.6%	1.3%	4.7%	8.2%
FFV	0.210	0.211	0.213	0.221	0.241	0.281

4.5. Dynamics of PI and CO_2

The dynamics of PI chains and CO_2 molecules can be reflected by the mean-squared displacement (MSD). the MSD was calculated from MD trajectory

$$\left\langle r^2(t)\right\rangle = \frac{1}{N}\sum_{i=1}^{N}\left\langle \left|r_i(t)-r_i(0)\right|^2\right\rangle \tag{6}$$

where $r_i(t)$ is the position of the ith atom at time t and brackets denotes the ensemble average. To improve statistical accuracy, the multi-time origin method was used to calculate the MSD. The PI backbone is composed primarily of aromatic carbon atoms; therefore, the MSD of these atoms was used to examine the dynamics of PI chains. At low loadings with 5, 10, and 20 CO_2 molecules shown in Fig. 8, the MSDs are almost flat within 9 ns MD run, which implies a small mobility of the polymer chains. As the loading increases to 40 and 80, the mobility is enhanced. This is

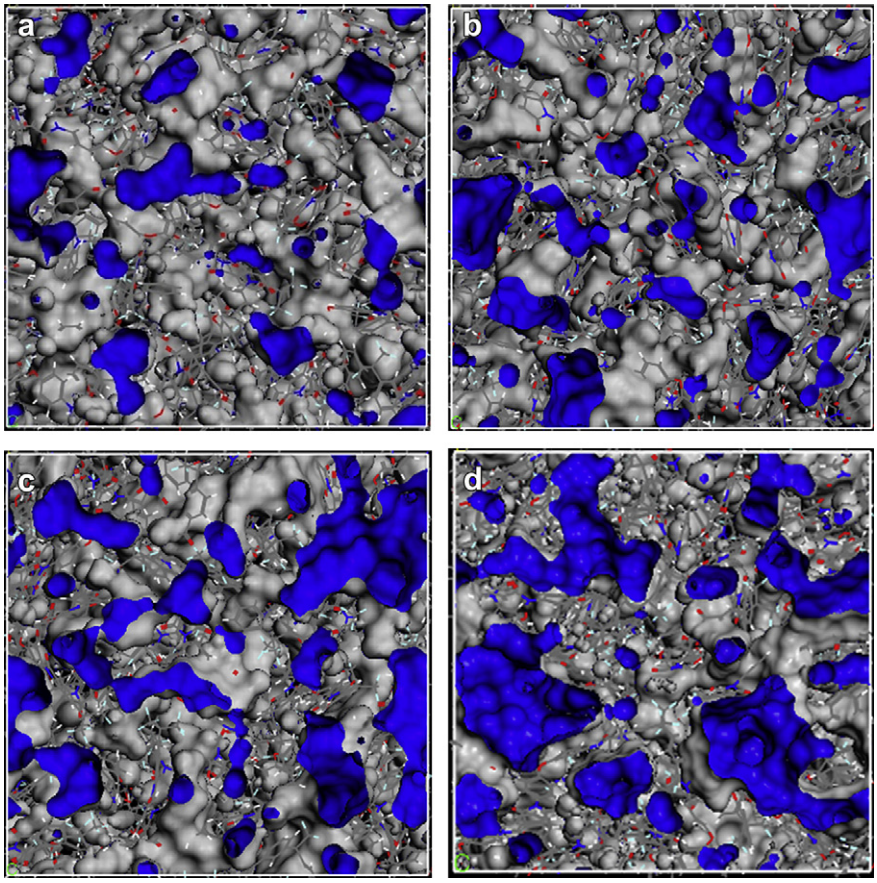

Fig. 5. Morphology of free volume in (a) PI and (b–d) PI/CO_2 systems at different CO_2 loadings with 10, 20, 40, and 80 CO_2 molecules in the simulation cell.

because the sorbed CO_2 molecules swell polymer chains, leads to volume dilation and larger voids. The pronounced enhancement in the mobility at 40 CO_2 loading may suggest the incipient point of plasticization.

Fig. 9 shows the MSDs of CO_2 molecules in PI/CO_2 systems at different CO_2 loadings. The slight fluctuations near the end of 18 ns are due to the insufficient data for statistics. The CO_2 mobility in the PI membrane increases as CO_2 loading increases. At low loadings (e.g. 5 or 10 CO_2 molecules), CO_2 molecules are preferentially sorbed at the favorable sites and the volume dilation is negligible. In other words, CO_2 molecules are strongly trapped and the mobility is extremely small. When CO_2 loading increases, the favorable sites are saturated and more CO_2 molecules are bound at the relatively weak sites, resulting in a larger mobility. At the same time, because of the

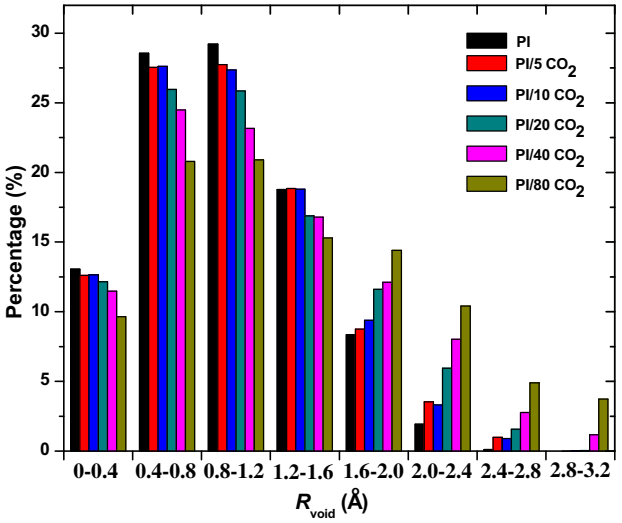

Fig. 6. Distributions of void radius in PI and PI/CO_2 systems at different CO_2 loadings with 5, 10, 20, 40, and 80 CO_2 molecules in the simulation cell.

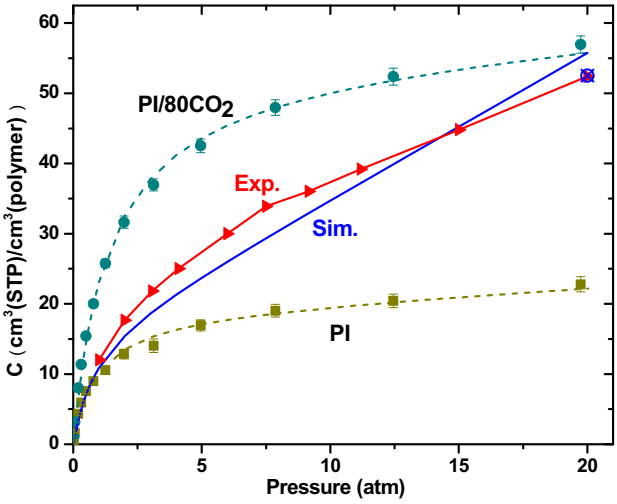

Fig. 7. Experimental and simulated CO_2 sorption isotherms at 308 K. The dotted lines are the fits of the dual-mode sorption model to the simulated isotherms in PI and PI/80CO_2 systems, respectively. The reference point from experiment at 20 atm is labeled by ⊠.

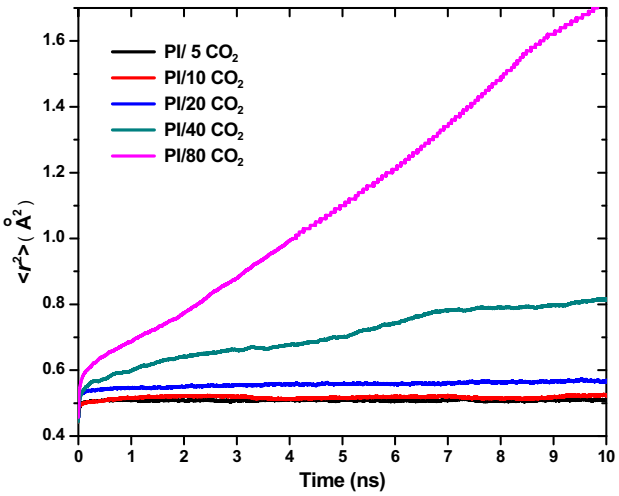

Fig. 8. Mean-squared displacements of polymer chains as a function of time in PI/CO_2 systems at different CO_2 loadings with 5, 10, 20, 40, and 80 CO_2 molecules in the simulation cell.

increasing interactions between CO_2 and polymer, the mobility of polymer chains increases, volume dilatation occurs, and larger voids appear; which in turn enhance CO_2 mobility. Similar to Fig. 8, a large magnitude of enhancement is seen in the MSD at a loading of 40 CO_2 molecules. The diffusion coefficient of CO_2 can be in-principle calculated using the Einstein relationship for normal diffusion, in which the MSD changes linearly with time in the logarithmic scale. Nevertheless, the polymer chains of the glassy PI membrane are rather rigid and the diffusion of CO_2 is largely retarded; consequently, CO_2 cannot reach normal diffusion within a nanosecond time scale. This is a common problem in molecular simulation studies to predict the diffusion coefficients in glassy membranes [28,31]; and advanced simulation technique is required. For example, the transition-state theory has been used; however, it is mostly applicable for spherical penetrants at infinite dilution.

The dynamic pattern of CO_2 molecule in the host PI membrane can be analyzed in detail by tracing its displacement and trajectory. Fig. 10a shows the displacement $|r(t) - r(0)|$ of a single CO_2 molecule during 18 ns MD run for different PI/CO_2 systems. The displacement represents a common hopping mechanism, showing that for a considerable time interval the CO_2 molecule is trapped in

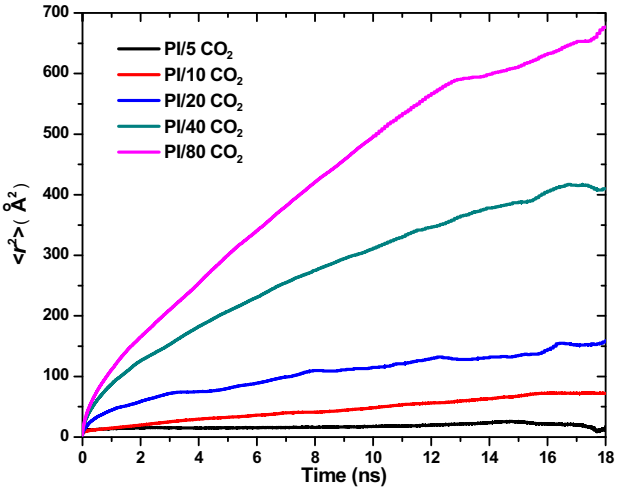

Fig. 9. Mean-squared displacements of CO_2 molecules as a function of time in PI/CO_2 systems at different CO_2 loadings with 5, 10, 20, 40, and 80 CO_2 molecules in the simulation cell.

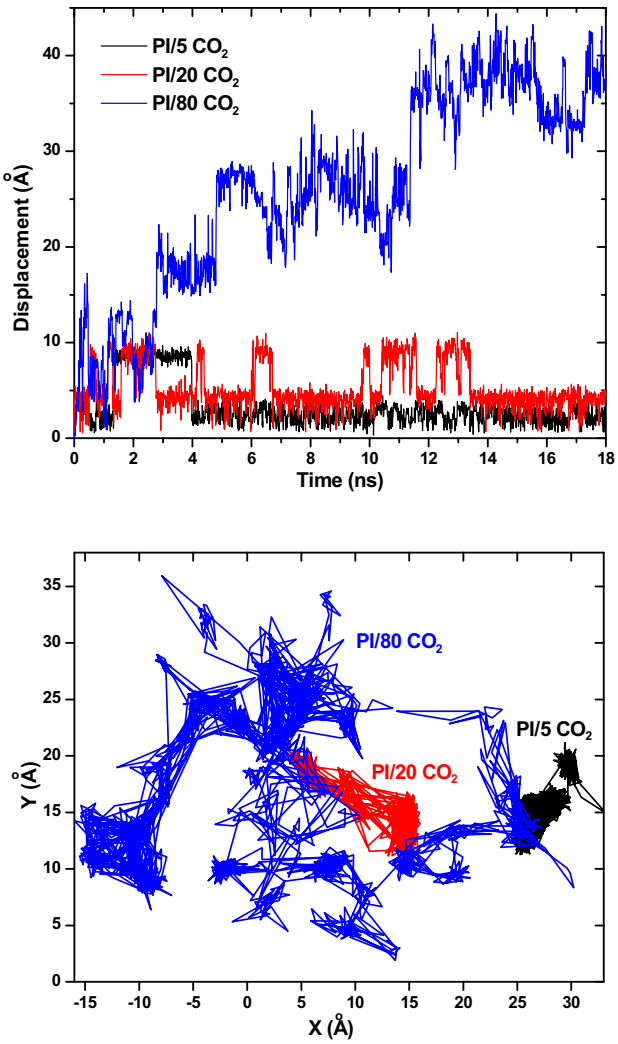

Fig. 10. (a) Displacement (b) X–Y trajectory of a single CO_2 molecule in PI/CO_2 systems at different CO_2 loadings with 5, 20, and 80 CO_2 molecules in the simulation cell.

a void and occasionally jumps into a neighboring void. The trapped CO_2 molecule exhibits oscillation and no net diffusion occurs. The jumping frequency depends on the dynamics of polymer segments and the inter-connection of voids. At a low loading with 5 CO_2 molecules, the CO_2 molecule selected for plot in Fig. 10a jumps only twice within 18 ns duration. The other four CO_2 molecules (not plotted) are trapped in their initial voids over the whole 18 ns. Fig. 10b shows the two-dimensional X–Y trajectory for the center-of-mass of the selected CO_2 molecule. Apparently, the CO_2 molecule is largely trapped and exhibits small mobility in either X or Y direction. With increasing to 20 CO_2 molecules, the CO_2 molecule jumps more frequently. At a much larger loading with 80 CO_2 molecules, the jumping motion is significantly enhanced, as reflected in the higher frequency and longer distance. This reveals the existence of larger and more continuous voids at a higher CO_2 loading, as discussed in Figs. 4–6, which provide more free space for CO_2 to diffuse. In addition, we find that the oscillation of CO_2 when trapped in a void is related to the void size. At a high loading, the oscillation amplitude is greater because of the larger voids present in the polymer matrix.

Generally, the dynamics of gas molecules in a polymer matrix are classified into three types, namely, trapped, jumping, and continuous motions [45]. To further unravel the mechanism of CO_2 in a PI/CO_2 system, the percentages of these three different motions

Table 2
Percentages of jumping, trapped, and continuous motions of CO_2 in PI/CO_2 systems at different CO_2 loadings with 5, 10, 20, 40, and 80 CO_2 molecules in the simulation cell.

	PI/5 CO_2	PI/10 CO_2	PI/20 CO_2	PI/40 CO_2	PI/80CO2
$P_{jumping}$	0.38	0.78	1.53	2.31	2.21
$P_{trapped}$	91.61	88.09	84.15	74.79	69.58
$P_{continuous}$	8.01	11.13	14.32	22.90	28.21

were estimated on the basis of CO_2 displacement. More specifically, if the displacement in a 1-ps duration was larger than the average diameter of the voids, the motion was classified as jumping. Next, five subsequent displacements were fitted to a linear line and if the slope of the line was less than 0.05 Å/ps, the motion was regarded as trapped [46,47]. The percentages of the jumping and trapped motions were counted in the whole trajectory, and the rest was the continuous motion. Table 2 gives the time-averaged percentages of jumping, trapped, and continuous motions of CO_2 in PI/CO_2 systems at different CO_2 loadings. The percentage of jumping motion is rather small compared to the other two motions, and increases slightly from low loadings but tends to remain as a constant at high loadings. While the percentage of the continuous motion increases with increasing CO_2 loading, the opposite is true for the trapped motion. The jumping and continuous motions are considered to be effective in diffusion, and their overall percentages increase monotonically as CO_2 loading increases. Therefore, as seen in Figs. 9 and 10, CO_2 diffusion is enhanced with increasing loading and the primary contribution is the continuous motion.

5. Conclusions

We have investigated CO_2-induced plasticization in 6FDA-ODA polyimide membrane by combining experimental and simulation techniques. As found from experiments, the diffusion coefficient of CO_2 increases with increasing pressure, in contrast to the solubility coefficient. The permeability exhibits a minimum at a plasticization pressure of 8 atm. The general feature of experimental sorption isotherm is captured well by simulation. Because of the differences in sorption process and model used, however, deviations are observed between experiments and simulation. From the simulated structure analysis, the initial CO_2 sorption occurs preferentially at the imide groups, and then at the ether and CF_3 groups with increasing CO_2 loading. At high pressures, the interactions of CO_2 with the ether groups have a stronger effect on the mobility of polyimide chains. Therefore, we suggest that a polymer with fewer ether groups could suppress the plasticization induced by CO_2 sorption.

At low loadings, CO_2 molecules are largely trapped by the voids in the polymer matrix and have small mobility. With increasing loading, CO_2 molecules jump more frequently with higher frequency and longer distance. The percentage of jumping motion is small and varies marginally with loading. CO_2 diffusion is contributed primarily from the continuous motion, which increases in percentage as CO_2 loading increases. The polyimide chains are swollen gradually upon increase of CO_2 loading and show enhanced mobility. This leads significantly to the depression of glass transition temperature, volume dilation, increase of fractional free volume, and appearance of large voids. The glass transition temperature of the polyimide is 589 K, and reduces to 583, 582, 571, 543, 522 K with CO_2 loadings of 5, 10, 20, 40, and 80, respectively. The volume dilation is small at low loadings, but increases with loading. Small voids prevail dominantly in the polymer matrix at low loadings; however, larger and interconnected voids are observed at high loadings. The mean radius of voids increases from 2.5 to 3.3 Å with increasing CO_2 loading. There is a pronounced enhancement in the mobility of both CO_2 molecules and polyimide chains when CO_2 loading approaches 40, which might be the incipient point of plasticization. The mechanistic understanding of CO_2-induced plasticization in the polyimide membrane from a microscopic level is critical to the new development of high-performance polymeric membranes.

Acknowledgment

The authors are grateful for the support from the Singapore National Research Foundation on the Competitive Research Programme (R-279-000-261-281).

References

[1] Kazarian SG, Vincent MF, Bright FV, Liotta CL, Eckert CA. J Am Chem Soc 1996;118:1729–36.
[2] Ismail AF, Lorna W. Sep Purif Technol 2002;27:173–94.
[3] Shieh YT, Su JH, Manivannan G, Lee PHC, Sawan SP, Spall WD. J Appl Polym Sci 1996;59:707–17.
[4] Chiou JS, Barlow JW, Paul DR. J Appl Polym Sci 1985;30:2633–42.
[5] Handa YP, Capowski S, Oneill M. Thermochim Acta 1993;226:177–85.
[6] Pissis P, Apekis L, Christodoulides C, Niaounakis M, Kyritsis A, Nedbal J. J Polym Sci Pt B-Polym Phys 1996;34:1529–39.
[7] Hodge RM, Bastow TJ, Edward GH, Simon GP, Hill AJ. Macromolecules 1996; 29:8137–43.
[8] Okamoto KI, Tanihara N, Watanabe H, Tanaka K, Kita H, Nakamura A, et al. J Polym Sci Pt B-Polym Phys 1992;30:1223–31.
[9] Wang BG, Yamaguchi T, Nakao SI. J Polym Sci Pt B-Polym Phys 2000;38:846–56.
[10] Briscoe BJ, Kelly CT. Polymer 1995;36:3099–102.
[11] Wind JD, Paul DR, Koros WJ. J Membr Sci 2004;228:227–36.
[12] Park HB, Jung CH, Lee YM, Hill AJ, Pas SJ, Mudie ST, et al. Science 2007;318:254–8.
[13] Lin HQ, Van Wagner E, Freeman BD, Toy LG, Gupta RP. Science 2006;311:639–42.
[14] Chiou JS, Paul DR. J Membr Sci 1987;32:195–205.
[15] Kamiya Y, Hirose T, Naito Y, Mizoguchi K. J Polym Sci Pt B-Polym Phys 1988; 26:159–77.
[16] Sanders ES. J Membr Sci 1988;37:63–80.
[17] Bos A, Punt IGM, Wessling M, Strathmann H. J Membr Sci 1999;155:67–78.
[18] Xiao YC, Low BT, Hosseini SS, Chung TS, Paul DR. Prog Polym Sci 2009;34:561–80.
[19] Wind JD, Sirard SM, Paul DR, Green PF, Johnston KP, Koros WJ. Macromolecules 2003;36:6433–41.
[20] Wessling M, Huisman I, Vanderboomgaard T, Smolders CA. J Appl Polym Sci 1995;58:1959–66.
[21] Hong X, Jean YC, Yang H, Jordan SS, Koros WJ. Macromolecules 1996;29:7859–64.
[22] Kamiya Y, Mizoguchi K, Hirose T, Naito Y. J Polym Sci Pt B-Polym Phys 1989; 27:879–92.
[23] Wessling M, Borneman Z, Vandenboomgaard T, Smolders CA. J Appl Polym Sci 1994;53:1497–512.
[24] Zhou C, Chung TS, Wang R, Liu Y, Goh SH. J Membr Sci 2003;225:125–34.
[25] Duthie X, Kentish S, Powell C, Nagai K, Qiao G, Stevens G. J Membr Sci 2007;294:40–9.
[26] Chung TS, Cao C, Wang R. J Polym Sci Pt B-Polym Phys 2004;42:354–64.
[27] Chern RT, Provan CN. Macromolecules 1991;24:2203–7.
[28] Hofmann D, Fritz L, Ulbrich J, Schepers C, Bohning M. Macromol Theory Simul 2000;9:293–327.
[29] van der Vegt NFA, Briels WJ, Wessling M, Strathmann H. J Chem Phys 1999; 110:11061–9.
[30] Holck O, Siegert MR, Heuchel M, Bohning M. Macromolecules 2006;39:9590–604.
[31] Heuchel M, Boehning M, Holck O, Siegert MR, Hofmann D. J Polym Sci Pt B-Polym Phys 2006;44:1874–97.
[32] Holck O, Heuchel M, Bohning M, Hofmann D. J Polym Sci Pt B-Polym Phys 2008;46:59–71.
[33] Spyriouni T, Boulougouris GC, Theodorou DN. Macromolecules 2009;42:1759–69.
[34] Materials studio 4.3 edition. San Diego: Accelrys; 2008.
[35] Tanaka K, Kita H, Okano M, Okamoto K. Polymer 1992;33:585–92.
[36] Hofmann D, Heuchel M, Yampolskii Y, Khotimskii V, Shantarovich V. Macromolecules 2002;35:2129–40.
[37] Ban S, Vlugt TJH. Mol Simul 2009;35:1105–15.
[38] Bhattacharya S, Gubbins KE. Langmuir 2006;22:7726–31.
[39] Sun H, Mumby SJ, Maple JR, Hagler AT. J Am Chem Soc 1994;116:2978–87.
[40] Sun H. J Phys Chem B 1998;102:7338–64.
[41] Smith W, Forester TR. J Mol Graph 1996;14:136–41.
[42] Smith W, Yong CW, Rodger PM. Mol Simul 2002;28:385–471.
[43] Cohen MH, Turnbull D. J Chem Phys 1959;31:1164–9.
[44] Chapman BR, Gochanour CR, Paulaitis ME. Macromolecules 1996;29:5635–49.
[45] Smit E, Mulder FM, Smolders CA, Karrenbeld H, vE J, Feil D. J Membr Sci 1992; 73:247.
[46] Chang KS, Tung CC, Wang KS, Tung KL. J Phys Chem B 2009;113:9821–30.
[47] Chang KS, Hsiung CC, Lin CC, Tung KL. J Phys Chem B 2009;113:10159–69.